# Chapter II.5
# Electrochemical Impedance Spectroscopy

**Utz Retter and Heinz Lohse**

## II.5.1 Introduction

Non-steady-state measuring techniques are known to be extremely suitable for the investigation of the electrode kinetics of more complex electrochemical systems. Perturbation of the electrochemical system leads to a shift of the steady state. The rate at which it proceeds to a new steady state depends on characteristic parameters (reaction rate constants, diffusion coefficients, charge transfer resistance, double-layer capacity). Due to non-linearities caused by the electron transfer, low-amplitude perturbation signals are necessary. The small perturbation of the electrode state has the advantage that the solutions of relevant mathematical equations used are transformed in limiting forms that are normally linear. Impedance spectroscopy represents a powerful method for investigation of electrical properties of materials and interfaces of conducting electrodes. Relevant fields of application are the kinetics of charges in bulk or interfacial regions, the charge transfer of ionic or mixed ionic–ionic conductors, semiconducting electrodes, the corrosion inhibition of electrode processes, investigation of coatings on metals, characterisation of materials and solid electrolyte as well as solid-state devices.

## II.5.2 Definitions, Basic Relations, the Kramers–Kronig Transforms

If a monochromatic alternating voltage $U(t) = U_\mathrm{m} \sin(\omega t)$ is applied to an electrode then the resulting current is $I(t) = I_\mathrm{m} \sin(\omega t - \vartheta)$ where $\vartheta$ is the phase difference between the voltage and the current and $U_\mathrm{m}$ and $I_\mathrm{m}$ are the amplitudes of the sinusoidal voltage and current, respectively. Then the impedance is defined as

$$Z = U(t)/I(t) = |Z| \, \mathrm{e}^{\mathrm{j}\vartheta} = Z' + \mathrm{j}Z'' \qquad \text{(II.5.1)}$$

U. Retter (✉)
Balzerstr. 45, 12683 Berlin, Germany
e-mail: Utz.Retter@gmx.de

F. Scholz (ed.), *Electroanalytical Methods*, 2nd ed.,
DOI 10.1007/978-3-642-02915-8_8, 

with

$$\mathrm{j} = (-1)^{1/2} \tag{II.5.2}$$

where $Z'$ and $Z''$ are the real and imaginary part of $Z$, respectively.

Impedance $Z$ and admittance $Y$ are related as follows:

$$Y = 1/Z = Y' + \mathrm{j}Y'' \tag{II.5.3}$$

Now let us sum up the following definitions: resistance: $Z'$ (also $R$), reactance: $Z''$ (also $X$), magnitude of impedance: $|Z|$, conductance: $Y'$ (also $G$), susceptance: $Y''$ (also $B$), quality factor: $Q = \left|Z''/Z'\right| = \left|Y''/Y'\right|$, dissipation factor: $D = 1/Q = |\tan\delta|$, loss angle: $\delta$.

$$|Z|^2 = \left(Z'\right)^2 + \left(Z''\right)^2 \tag{II.5.4}$$

$$\delta = \arctan\left(Z'/Z''\right) \tag{II.5.5}$$

Frequently used procedures in modelling include the conversion of a parallel circuit to a series one and the conversion of a series circuit to a parallel one.

The series circuit and the parallel circuit must be electrically equivalent. This means the dissipation factors $|\tan\delta|$ must be the same and the absolute values $|Z| = 1/|Y|$.

The following equations enable these procedures to be performed [1]:

$$\begin{aligned} &\tan\delta = \cot\vartheta = Z'/Z'' = -Y'/Y'' \text{ and} \\ &|Z|^2 = 1/|Y|^2 = \left(Z'\right)^2 + \left(Z''\right)^2 = 1/\left(\left(Y'\right)^2 + \left(Y''\right)^2\right) \end{aligned} \tag{II.5.6}$$

For an $RC$ circuit with components $R_\mathrm{s}$, $C_\mathrm{s}$ (series) and $R_\mathrm{par}$, $C_\mathrm{par}$ (parallel), the following relations are valid:

$$\begin{aligned} Z' &= R_\mathrm{s}, \\ Z'' &= -1/(\omega C_\mathrm{s}), \\ Y' &= 1/R_\mathrm{par}, \\ Y'' &= \omega C_\mathrm{par} \end{aligned} \tag{II.5.7}$$

$$R_\mathrm{par} = R_\mathrm{s}\left(1 + 1/\tan^2\delta\right) \tag{II.5.8}$$

$$C_\mathrm{par} = C_\mathrm{s}/\left(1 + \tan^2\delta\right) \tag{II.5.9}$$

The Kramers–Kronig frequency domain transformations enable the calculation of one component of the impedance from another or the determination of the phase angle from the magnitude of the impedance or the polarization resistance $R_\mathrm{p}$ from the imaginary part of the impedance. Furthermore, the Kramers–Kronig (KK) transforms allow the validity of an impedance data set to be checked. Precondition for the application of KK transforms is, however, that the impedance must be finite-valued

for the limits $\omega \to 0$ and $\omega \to \infty$, and must be a continuous and finite-valued function at all intermediate values.

Let us now sum up the KK transforms:

$$Z'(\omega) - Z'(\infty) = (2/\pi) \int_0^\infty \left[ \left( xZ''(x) - \omega Z''(\omega) \right) / \left( x^2 - \omega^2 \right) \right] \mathrm{d}x \tag{II.5.10}$$

$$Z'(\omega) - Z'(0) = (2\omega/\pi) \int_0^\infty \left[ \left( (\omega/x)\, Z''(x) - Z''(\omega) \right) / \left( x^2 - \omega^2 \right) \right] \mathrm{d}x \tag{II.5.11}$$

$$Z''(\omega) = -(2\omega/\pi) \int_0^\infty \left[ \left( Z'(x) - Z'(\omega) \right) / \left( x^2 - \omega^2 \right) \right] \mathrm{d}x \tag{II.5.12}$$

$$\vartheta\,(\omega) = (2\omega/\pi) \int_0^\infty \left[ (\ln |Z\,(x)|) / \left( x^2 - \omega^2 \right) \right] \mathrm{d}x \tag{II.5.13}$$

$$R_\mathrm{p} = (2/\pi) \int_0^\infty \left[ \left( Z''(x) \right) / x \right] \mathrm{d}x \tag{II.5.14}$$

## II.5.3 Measuring Techniques

The measuring principle is simple. On an electrochemical system in equilibrium a small signal acts (time-dependent potential or current). The response of the system is measured then. "Small signal" means the perturbation of the system is so low that the response is linear, i.e. harmonic generation and frequency mix products can be neglected. The signal can be a single sinus wave or consist of a sum of such waves with different amplitudes, frequencies and phases (e.g. single potential or current step, pulse-shaped signals, noise). In the majority of cases, electrochemical systems are linear at signal amplitudes of 10 mV or less. On application of a sum signal, the effective value of the signal must keep that condition. The overall equivalent circuit at high frequencies can be assumed as a series combination of the linear solution resistance and the predominantly capacitive interface. Then, only a part of the amplitude applied to the electrochemical cell is applied to the interface because most of the potential drop occurs at the solution resistance. Therefore, the signal amplitude can be chosen higher without violating the linearity conditions. One can check the validity of the linearity condition by checking the independence of the impedance on the test signal amplitude.

The input signal can be a single frequency, a discrete number of frequencies (e.g. computer generated) or a theoretical unlimited spectrum of frequencies (white noise). Primarily, it seems of advantage to apply a large number of frequencies and measure the response simultaneously. However, the electrochemical system generates noise and, because of the linearity condition, the signal amplitudes are very

small. Therefore, a signal averaging must be used for the response signal. This is very time consuming, mainly for low frequencies and high impedances.

In time-domain measurements the test signal has a time-dependent shape (ramp function, triangle or square pulse) and the time dependence of the system response is measured. From the time dependence of the signal response, information can be obtained about the system parameters but their extraction is very complicated or impossible for non-trivial systems. Data transition from the time domain into the frequency domain and back can be made with transform methods. Commercial measuring systems use fast Fourier transformation (FFT). The use of FFT is recommended in the low frequency region ($10^{-3}$ – $10^{2}$ Hz) because the cycle duration of the highest signal frequency is large in comparison to the conversion time of the precision analog-to-digital converters (ADC) and FFT speed. Digital signal filtering is here superior to analog filters. The measuring methods for system response are physically equivalent (same limitations in noise-bandwidth) but different methods can be suited more or less in dependence of the system under investigation and the hard- and software used in the measuring system.

Frequency analysis (measuring in frequency domain) can be used over a very large frequency range ($10^{-3}$ – $10^{7}$ Hz). Normally, a single frequency signal is used and the amplitude and phase shift, or real and imaginary parts of response signal, is measured [2]. Figure II.5.1 shows a block diagram of a potentiostatic frequency response analyser.

In commercial impedance analysers, commonly the polarization and the test signals are generated separately. The polarization is a large-scale signal and the requirements on electrical circuits as amplifiers and digital-to-analog converters (DAC) are: high constant system parameters in time and temperature and precise amplitude and low noise characteristic over the whole potential region (e.g. $\pm$ 5 V in 1 mV steps). The system for generating the test signal (small signal) must be

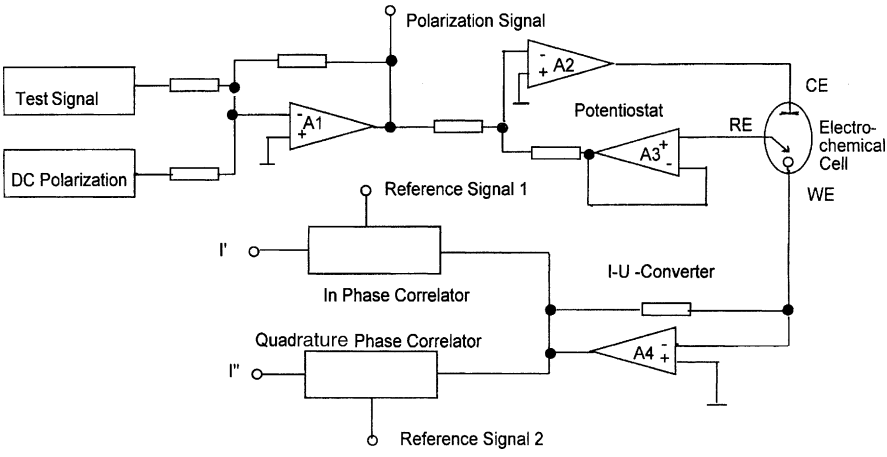


**Fig. II.5.1** Block diagram of a potentiostatic frequency response analyser

linear over the entire frequency and amplitude scale and the noise amplitude must be low too. The sum of signals at the output of the operations amplifier A1 is the polarization signal of the electrochemical cell. The amplifiers A2 and A3 together with the cell compose a potentiostat. The potential of the reference electrode (RE) is compared with the polarization signal and the control loop with A2 changes the potential at the counter electrode (CE) until the potential at RE is equal the sum from the test signal and the DC polarization signal. An important problem for measuring the impedance behaviour at high frequencies is the influence of parasitic elements and the phase shift connected with the potentiostatic control of the system. In the worst case the system can oscillate. However, before oscillations occur, the phase shifts and variations of the amplitude of the response signals give incorrect impedance values. Then, a precise dummy cell with well-known parameters similar to the cell impedance should be measured to examine it. For cases without or very small direct current, a two-electrode configuration can be used to avoid problems with phase shifts. Then the RE is connected to the CE and the amplifier A3 can be replaced with a resistor.

The decoupling of ac and dc signals is another way to avoid phase shifts and amplitude deformations at high frequencies. The cut-off frequency of the potentiostat is then far lower than the cycle duration of the ac signal [3]. In Fig. II.5.1 the output potential of the amplifier A4 is proportional to the cell current (*I*-*U* converter). Here, the input potential of A4 is controlled to be zero (virtual earth) and there are no additional parasitic impedance elements in the measuring circuit. In the case of high cell currents and for very high frequencies, the *I*-*U* converter can show non-ideal behaviour. Then, the current can be measured by determining the potential drop on a small resistance between the working electrode and the earth. The output signal of A4 is applied to a phase sensitive detector. Here, it is compared with reference signals 1 and 2 in phase or 90° shifted to the test signal, respectively. As a result, the output signals $I'$ and $I''$ are proportional to the in-phase and quadrature components of the cell current. Some analysers determine the amplitude and phase of the response signal. The results are equivalent and the inherent problems are the same. At high frequencies and/or if $I'$ and $I''$ are very different (phase angle $\approx 0°$ or $\approx -90°$), the phase discriminators show a "cross talk" effect, e.g. the component with the high amplitude influences the other. Generally, the precision of the phase angle is lower at higher frequencies.

An impedance spectrum is the result of a sweep about the selected frequency band. Narrow band measuring (filters or lock-in amplifiers) is able to improve the accuracy and sensitivity but it is time consuming at low frequencies. For precise measurements (suppressing of transients), a signal averaging at least five periods is recommended.

Broadband perturbing signals used in connection with frequency transformation (mostly FFT algorithm) can allow a faster measuring in time-varying systems. However, an increase in speed decreases the accuracy and deteriorates the signal-to-noise ratio. To improve this ratio signal accumulation must be performed and the gain in measuring time is lost. A special method to measure the impedance or admittance of an electrochemical system is to compare its signal response with

the response of a combination of calibrated impedance elements (use of audio- and radio-frequency bridges or substitution methods). Here, the accuracy of the method is only affected by the elements and the sensitivity and stability of the amplitude and phase measuring. The handicap here is that the method is very time consuming. Time domain techniques mostly use step and ramp signals.

For electrochemical impedance spectroscopy a number of excellent commercial measuring systems exist. In some cases it is favourable to use precision impedance analysers designed specially for accurate impedance measurements of electronic components and materials in a broad-frequency scale.

## II.5.4 Representation of the Impedance Data

The impedance data will be represented in complex plane plots as $-Z''$ vs. $Z'$ (normally called the Nyquist diagrams), $Y''$ vs. $Y'$ diagrams and derived quantities as the modulus function $M = \mathrm{j}\omega C_C Z = M' + \mathrm{j}M''$ ($C_C$ is the capacity of the empty cell) and the complex dielectric constant $\varepsilon = 1/M = \varepsilon' - \mathrm{j}\varepsilon''$ depictions. Frequently used terms are as follows: the complex plane plot of the frequency normalized admittance components $Y'/\omega$ vs. $Y''/\omega$ specially for an investigation of non-faradaic processes (the frequency acts as parameter) and the Bode plot for the representation of the magnitude of impedance $|Z|$ and the phase angle $\vartheta$ vs. $\log \nu$, ($\nu$ being the measuring frequency). It should be noted that the representation form and any mathematical transformation can never improve the quality of the data fitting, i.e. the fitting should always start with the experimental data.

## II.5.5 Equivalent Circuits

Any electrochemical cell can be represented in terms of an equivalent electrical circuit that comprises a combination of resistances, capacitances or inductances as well as mathematical components. At least the circuit should contain the double-layer capacity, the impedance of the faradaic or non-faradaic process and the high-frequency resistance. The equivalent circuit has the character of a model, which more or less precisely reflects the reality. The equivalent circuit should not involve too many elements because then the standard errors of the corresponding parameters become too large (see Sect. II.5.7), and the model considered has to be assessed as not determined, i.e. it is not valid.

## II.5.6 The Constant Phase Element

For an ideally polarized electrode, the impedance consists of the double-layer capacity $C_d$ and the solution resistance $R_\Omega$ in series. In the impedance plane plot, a straight vertical line results intersecting the $Z'$-axis at $Z' = R_\Omega$. At solid electrodes, especially

due to contamination and roughness, a straight line can be observed intersecting the $Z'$-axis at $R_\Omega$ at an angle smaller than 90° to the real axis. The corresponding phase angle $\vartheta_C = -(1-\beta)\,\pi/2$ is assumed to be independent of frequency, i.e. a "constant phase angle" occurs [4, 5] and, consequently, the impedance follows as

$$Z = R_\Omega + Z_C = R_\Omega \left[1 + (j\omega\tau)^{-(1-\beta)}\right] \tag{II.5.15}$$

where $\tau = R_\Omega C_d$. The dimensionless parameter $\beta$ ranges between 0 and 1. For $\beta = 0$, the well-known case of a series connection of $R_\Omega$ and $C_d$ follows. If the electrode consists of $R_\Omega$ in series with an impedance $Z_C$ with a constant-phase angle (the "constant-phase element", CPE), $C_d$ will be replaced by the CPE. As a consequence, the corresponding admittance changes from a semicircular arc to a depressed semicircular arc.

$$Y = 1/Z = (1/R_\Omega)\left[1 - 1/\left(1 + (j\omega\tau)^{(1-\beta)}\right)\right] \tag{II.5.16}$$

When a charge transfer proceeds at the electrode, the equivalent circuit consists of $C_d$ and the charge-transfer resistance $R_{ct}$ in parallel. Therefore, the corresponding Nyquist impedance plot represents a semicircular arc. Analogous to the case just considered above, a replacement of $C_d$ by the CPE leads to a change from a semicircular arc to a depressed semicircular arc.

A full discussion of the distribution of relaxation times as the origin of constant-phase elements is available in the literature [5].

In another report [4], an error in the interpretation of the CPE is pointed out. On the one hand, the double-layer capacity is replaced by the CPE, i.e. the CPE is a property of the double layer itself. On the other, the CPE is discussed as originating from surface inhomogeneities.

## II.5.7 Complex Non-Linear Regression Least-Squares (CNRLS) for the Analysis of Impedance Data

Let us consider a set of data $Z_i'$ and $Z_i''$. The measurements were performed at the angular frequencies $\omega_i$ $(i = 1 \ldots K)$. The theoretical values are denoted by $Z_{it}$ $(\omega_i, P_1, P_2 \ldots P_m)$, where $P_1$, $P_2 \ldots P_m$ are parameters to be determined and $m$ is the number of parameters. Such parameters can be rate constants, the charge transfer resistance, the double-layer capacity or the high-frequency resistance. The aim of the complex least-squares analysis consists of minimising the sum $S$:

$$S = \sum_{i=1}^{K} \left\{ \left[Z_i' - Z_{it}'\,(\omega_i, P_1, P_2, \ldots P_m)\right]^2 + \left[Z_i'' - Z_{it}''\,(\omega_i, P_1, P_2, \ldots P_m)\right]^2 \right\} \tag{II.5.17}$$

For the minimizing procedure one uses normally the Marquardt algorithm [6, 7].

Good starting values of the parameter play an important role here. Otherwise the least-squares sum may converge to local minima instead of the absolute minimum or the sum may even diverge. One should not blindly accept a model and tentatively assume that it is correct. There are the following criteria to assess the validity of a model, which must be fulfilled simultaneously:

(a) Small relative standard deviations of the parameters, smaller than 30% [5]. Otherwise the corresponding parameters have to be removed from the model. One should not believe "The more parameters the better." Often a simplification of the model leads to success, or other models should be tested.
(b) Small relative residuals for the data points are demanded [8]. The overall standard deviation of the fit, $(S/2K)^{1/2}$, divided by the mean value of the measuring values, should not exceed 10% for a model. In some cases, there are several models with comparable standard error of the fit and of the parameters. In this case, additional dependencies have to be investigated. For instance, if the potential dependence of a parameter alone does not allow a decision as to which model is valid, then the concentration dependence should also be investigated. To sum up this section: non-linear regression is a necessary mathematical quality control of models. Abuse of non-linear regression can only lead to a modern sort of (electro)alchemy, absurdly based on high-tech measurements.

## II.5.8 Commercial Computer Programs for Modelling of Impedance Data

Several commercial computer programs for the modelling of impedance data currently exist. In the first operation, an adequate equivalent circuit can be created. The standard impedance elements used here are: resistance, capacity, inductance, constant-phase element, Warburg impedance (semi-infinite linear diffusion), Warburg impedance (semi-infinite hemispherical diffusion), finite-length diffusion for transmissive and reflective boundary conditions, impedance of porous electrodes, impedance for the case of rate control by a homogeneous chemical reaction. In the second operation, the validity of the impedance data is checked by the KK rule check (see Sect. II.5.2). As the third operation, the model parameters will be adapted to the measured data using the complex non-linear regression least-squares (CNRLS) fit. The last operation involves the representation of the experimental data and the optimized calculated data using plot diagrams. Here, most often the Bode plot and the Nyquist impedance plot are taken.

## II.5.9 Charge Transfer at the Electrode – the Randles Model

A quasi-reversible charge transfer is considered with $R_{ct}$ the charge-transfer resistance and $j_0$ the exchange current density:

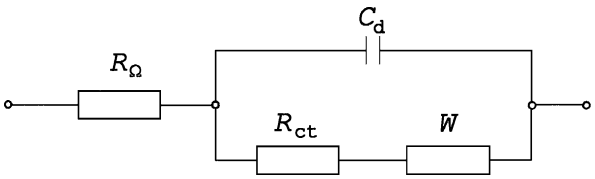


**Fig. II.5.2** Randles equivalent circuit

$$\mathrm{Ox} + n\mathrm{e} \rightarrow \mathrm{Red} \tag{II.5.18}$$

Let the species Ox and Red with concentrations $c_O$ and $c_R$ diffuse in the solution in the direction perpendicular to the electrode. $D_O$ and $D_R$ are the diffusion coefficients. The initial conditions demand that the solution is homogeneous and that the concentrations are equal to $c_O^*$ and $c_R^*$ for $t = 0$. Outside the Nernst layer the concentrations are equal to $c$, the concentrations in the bulk. At the electrode surface, the fluxes of Ox and Red are identical and equal to the normalized faradaic current $I_F/nFA$ ($A$: electrode area). The charge-transfer resistance $R_{ct}$ is defined as:

$$1/R_{ct} = (\delta I_F/\delta E)_c \tag{II.5.19}$$

$$k_f = k_f^0 \exp\left[-\alpha\,(nFE/RT)\right] \tag{II.5.20}$$

$$k_b = k_b^0 \exp\left[(1-\alpha)\,(nF/RT)\,E\right] \tag{II.5.21}$$

$$1/R_{ct} = \left(An^2F^2/RT\right)\left[ak_f c_O^* + (1-\alpha)\,k_b c_R^*\right] \tag{II.5.22}$$

$$R_{ct} = RT/\,(nFj_0) \tag{II.5.23}$$

where $\alpha$ is the apparent cathodic transfer coefficient and $j_0$ the exchange current density.

A quasi-reversible charge transfer is considered with the equivalent circuit shown in Fig. II.5.2.

Let us first consider the Randles model for higher frequencies. $R_\Omega$ is the high-frequency series resistance or electrolyte resistance and $C_d$ the double-layer capacity.

$$\begin{aligned} Z' &= R_\Omega + R_{ct}/\left(1+\omega^2C_d^2R_{ct}^2\right);\\ Z'' &= -\omega C_d R_{ct}^2/\left(1+\omega^2C_d^2R_{ct}^2\right) \end{aligned} \tag{II.5.24}$$

Rearranging, the equation gives

$$\left(Z' - R_\Omega - R_{ct}/2\right)^2 + \left(Z''\right)^2 = R_{ct}^2/4 \tag{II.5.25}$$

$$Z'' = -\left(Z' - R_\Omega\right)(\omega R_{ct}C_d) \tag{II.5.26}$$

This is the equation of a circle with its centre on the $Z'$-axis at $Z' = R_\Omega + 0.5\,R_{ct}$ and radius 0.5 $R_{ct}$. From the intersection point of the semicircle with the $R_s$-axis, one obtains the value $R_\Omega + R_{ct}$ and the high-frequency ohmic component is equal to $R_\Omega$. Let $\omega_{max}$ be the frequency at which $-Z''$ exhibits a maximum vs $Z'$. For the maximum of $-Z''$ it follows that:

$$\omega_{max} R_{ct} C_d = 1 \tag{II.5.27}$$

From the frequency at which $-Z''$ exhibits a maximum, $C_d$ can be estimated.

$$C_d = 1/\left(R_{ct}\omega_{max}\right) \tag{II.5.28}$$

The following problem arises in the interpretation of such semicircles in the complex plane impedance plots: every parallel combination of a constant resistance and constant capacity leads to a semicircle in the Nyquist plot of the impedance. To verify a charge transfer, for instance, the potential dependence of the charge-transfer resistance should be investigated to demonstrate the Butler–Volmer potential dependence of the exchange current.

Let us now consider a semi-infinite linear diffusion of charged particles from and to the electrode. The Faraday impedance is defined as the sum of the charge-transfer resistance $R_{ct}$ and the Warburg impedance $W$ corresponding to the semi-infinite diffusion of the charged particles

$$Z_F = R_{ct} + W \tag{II.5.29}$$

$$W = \left[R_{ct} K_W / \left(2\omega\right)^{1/2}\right](1 - j) \tag{II.5.30}$$

$$K_W = \left(k_{ox} / \left(D_O\right)^{1/2}\right) + \left(k_{red} / \left(D_R\right)^{1/2}\right) \tag{II.5.31}$$

Here, $k_{ox}$, $k_{red}$ are the rate constants for oxidation and reduction, respectively, and $D_O$ and $D_R$ are the diffusion coefficients of the oxidized and reduced reactants:

$$\sigma = K_W R_{ct} / \left(2\right)^{1/2} \tag{II.5.32}$$

where $\sigma$ is the Warburg coefficient. The Nyquist plot of $Z_W$ is a straight line at an angle of 45° to the real axis.

The complete Randles model includes mixed control by diffusion and charge transfer control.

The corresponding equations for $Z'$ and $Z''$ are [9, 10]

$$Z' = R_\Omega + \left(R_{ct} + \sigma\omega^{-1/2}\right)/Q_R \tag{II.5.33}$$

$$Z'' = -\left(\omega C_d \left(R_{ct} + \sigma\omega^{-1/2}\right)^2 + \sigma^2 C_d + \sigma\omega^{-1/2}\right)/Q_R \tag{II.5.34}$$

$$Q_R = \left(\sigma\omega^{1/2} C_d + 1\right)^2 + \omega^2 C_d^2 \left(R_{ct} + \sigma\omega^{-1/2}\right)^2 \tag{II.5.35}$$

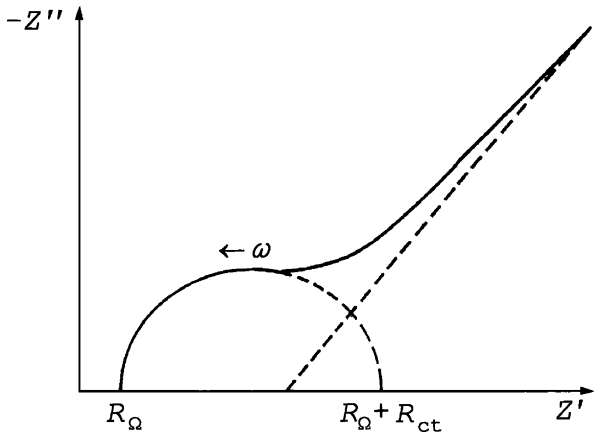


**Fig. II.5.3** Scheme of the impedance of the Randles equivalent circuit in the complex impedance plane (Nyquist plot)

Figure II.5.3 represents the Nyquist plot of the Randles impedance with the semicircle at higher frequencies and the straight line at an angle of 45° to the real axis at lower frequencies.

In the case of complex expressions for the impedance for more complicated electrochemical reactions, the calculations of the real and imaginary component can be very complicated. Then, it is much easier to split the whole calculation into elementary steps. We denote this method as cumulative calculation of the cell impedance. As an example, let us take again the Randles model.

The Warburg impedance is (see Eqs. II.5.30, II.5.31, and II.5.33)

$$\begin{aligned} W' &= \sigma\omega^{-1/2}; \\ W'' &= -\sigma\omega^{-1/2} \end{aligned} \tag{II.5.36}$$

In the first step, the charge-transfer resistance will be added

$$\begin{aligned} {Z_1}' &= W' + R_{\mathrm{ct}}; \\ {Z_1}'' &= W'' \end{aligned} \tag{II.5.37}$$

The second step involves a conversion from a series to a parallel circuit:

$$\text{Series in parallel: } \left({Z_1}', {Z_1}''\right) \rightarrow \left(1/R_{\mathrm{par2}}, C_{\mathrm{par2}}\right) \tag{II.5.38}$$

In the third step, the double-layer capacity $C_{\mathrm{d}}$ is added:

$$\begin{aligned} C_{\mathrm{par2}} + C_{\mathrm{d}} &= C_{\mathrm{par3}}; \\ R_{\mathrm{par2}} &= R_{\mathrm{par3}} \end{aligned} \tag{II.5.39}$$

The fourth step includes a conversion from a parallel to a series circuit:

$$\text{Parallel in series: } \left(R_{\mathrm{par3}}, C_{\mathrm{par3}}\right) \rightarrow \left(R_{\mathrm{s4}}, 1/\omega C_{\mathrm{s4}}\right) \tag{II.5.40}$$

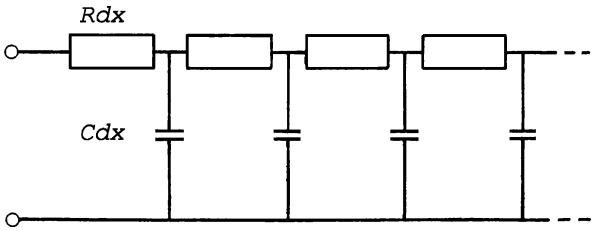


**Fig. II.5.4** Resistive-capacitive semi-infinite transmission line – the equivalent circuit for semi-infinite diffusion. R and C are normalized to unit length

In the fifth step, the high-frequency series resistance will be added:

$$\begin{aligned} R_{s4} + R_\Omega &= R_{s5}; \\ 1/\omega C_{s4} &= 1/\omega C_{s5} \end{aligned} \tag{II.5.41}$$

Now a direct modelling of the experimentally measured impedance data is possible due to comparison of $R_{s5}$ with $R_{s,exp}$ and $C_{s5}$ with $C_{s,exp}$.

The use of subroutines $(\bar{Z}'; \bar{Z}'') \rightarrow (\bar{Y}'/\omega; \bar{Y}''/\omega)$ and $(\bar{Y}'/\omega; \bar{Y}''/\omega) \rightarrow (\bar{Z}'; \bar{Z}'')$ makes the calculations much easier because now the calculations are reduced to repeating conversions of series components in parallel ones, and vice versa, and additions of the relevant parameters.

Equation (II.5.36) shows that the Warburg impedance cannot be represented as a series combination of frequency-independent elements in an equivalent circuit. This is possible, however, by a semi-infinite resistive-capacitive transmission line with a series resistance $R$ per unit length and a shunt capacity $C$ per unit length (Fig. II.5.4).

## II.5.10 Semi-infinite Hemispherical Diffusion for Faradaic Processes

The Warburg impedance for hemispherical diffusion corresponds to that of planar diffusion; however, with a resistance $\bar{R}_{par}'$ in parallel [10]. $1/\bar{R}_{par}'$ is inversely proportional to the mean size of the active centres. $1/\bar{R}_{par}'$ can be determined by representing $1/R_{par}$ vs. $(\omega)^{1/2}$. This gives a straight line with the intersection point for $\omega \rightarrow 0$ equal to $1/\bar{R}_{par}'$. According to Vetter [11], hemispherical diffusion occurs if the electrode surface is energetically inhomogeneous and the diffusion wavelength $l_d = (2D/\omega)^{1/2}$ is larger than $r_a$, the mean size of the active centres, but smaller than $r_i$, the mean size of the inactive centres. So an inhibiting film at the electrodes with proper sizes of pores leads to a hemispherical diffusion of the reacting ion. Indeed, such an effect was verified for the $Tl^+/Tl(Hg)$ electrode reaction in the presence of adsorbed tribenzylamine (TBA) condensed film [12]. The evaluation of the impedance data resulted in the sizes of active and inactive centres of the electrode,

which are, for $0.5 \times 10^{-4}$ M TBA, for instance, equal to 0.7 μm and 3.4 μm, respectively.

## II.5.11 Diffusion of Particles in Finite-Length Regions – the Finite Warburg Impedance

The infinite-length Warburg impedance obtained from solution of Fick's second law for one-dimensional diffusion considers the diffusion of a particle in semi-infinite space. Diffusion in the finite-length region is much more real. The thickness of the electrode or of a diffusion layer plays an important role then. In the case of a supported electrolyte, the thickness of the Nernst diffusion layer determines the finite length. In the case of an unsupported electrolyte, the finite length of solid electrolytes is decisive. Let the diffusion length be much less than the region available for diffusion then the case of infinite-length Warburg impedance is realized. When the diffusion length approaches the thickness of the diffusion region for decreasing frequencies, the shape of the complex plane impedance changes from 45° straight-line behaviour. Unhindered disappearance of diffusion at the far end due to contact with a conductor leads to a parallel combination of capacity $C_l$ and diffusion resistance $R_d$ at low frequencies, i.e. to a semicircle in the complex plane impedance plot (Fig. II.5.5).

From $C_l$, $R_d$ and the diffusion coefficient $D$, the thickness $l_d$ of the diffusion region can be obtained according to

$$C_l R_d = l_d^2/3D \tag{II.5.42}$$

This is denoted as diffusion for the transmissive boundary condition. The corresponding complete impedance is [5]

$$Z_{Wtr} = R_d \left[\tanh\left((js)^{1/2}\right) / (js)^{1/2}\right] \tag{II.5.43}$$

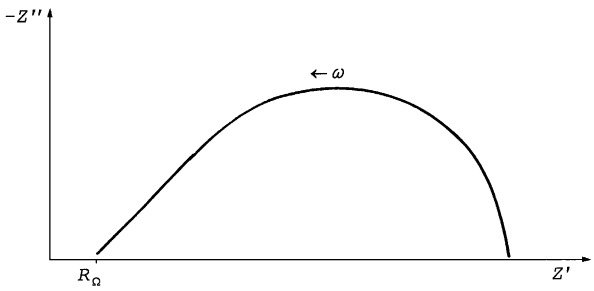


**Fig. II.5.5** Nyquist impedance plot due to finite length diffusion with a transmissive boundary condition

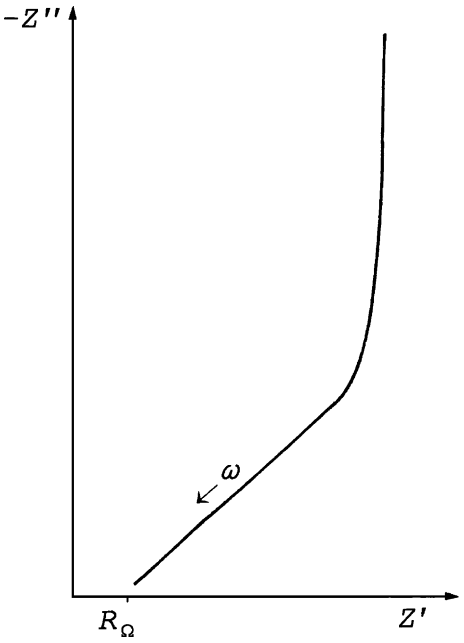


**Fig. II.5.6** Nyquist impedance plot due to finite-length diffusion with a reflective boundary condition

with

$$s = l_{\mathrm{d}}^2 \omega / D \tag{II.5.44}$$

An experimental example can be found in [13]. The diffusion coefficients of electrons and potassium ions in copper(II) hexacyanoferrate(II) composite electrodes were determined using impedance spectroscopy. Composite electrodes are mixtures of graphite and copper hexacyanoferrate (Cu hcf) powder embedded in paraffin. The diameter of the Cu hcf particles amounted to about 30 μm. The diffusion region of electrons is limited by the size of these particles. For the first time, a diffusion of electrons in hexacyanoferrates could be detected. The diffusion coefficient obtained was 0.1 $\mathrm{cm^2\ s^{-1}}$.

Let us now assume an open-circuit condition at the far end of the transmission line, i.e. no direct current can flow in the actual system. This is defined as diffusion in the case of the reflective boundary condition. At the far end complete blocking of diffusion occurs. This results in a vertical line at low frequencies in the Nyquist plot corresponding to a capacity only (Fig. II.5.6). Here, at very low frequencies, resistance $R_{\mathrm{d}}$ and capacity $C_{\mathrm{l}}$ are in series.

The complete expression for the Warburg impedance corresponding to finite diffusion with reflective boundary condition is [5]

$$Z_{\mathrm{Wr}} = (s/(\omega C_{\mathrm{l}})) \left[ \mathrm{ctnh}\left( (\mathrm{j}s)^{1/2} \right) / (\mathrm{j}s)^{1/2} \right] \tag{II.5.45}$$

## II.5.12 Homogeneous or Heterogeneous Chemical Reaction as Rate-Determining Step

According to Vetter [11, § 72], an electrochemical process can also be controlled by a chemical reaction in the bulk (homogeneous reaction) or at the interface (heterogeneous reaction). The corresponding expressions for the real and imaginary components of the impedance are presented for both cases in the paper by Vetter [11].

## II.5.13 Porous Electrodes

For porous electrodes, an additional frequency dispersion appears. First, it can be induced by a non-local effect when a dimension of a system (for example, pore length) is shorter than a characteristic length (for example, diffusion length), i.e. for diffusion in finite space. Second, the distribution characteristic may refer to various heterogeneities such as roughness, distribution of pores, surface disorder and anisotropic surface structures. De Levie used a transmission-line-equivalent circuit to simulate the frequency response in a pore where cylindrical pore shape, equal radius and length for all pores were assumed [14].

The impedance for pores is similar to that for diffusion in finite space [15]. Penetration into pores increases with decreasing frequency. The pore length determines the maximal possible penetration depth. The pore length plays the role of thickness in the case of finite space diffusion with reflective boundary condition. The diffusion is blocked at the end of the pore. At high frequencies, a straight line in the Nyquist plot follows with an angle of 45° to the real axis. For double-layer charging only, a vertical line in the Nyquist plot is predicted at low frequencies. For a charge transfer in the pores in addition to the double-layer charging, the low frequency part of the impedance corresponds to a semicircle.

Double-layer charging of the pores only (non-faradaic process) and inclusion of a pore-size distribution leads to complex plane impedance plots, as in Fig. II.5.7, i.e. at high frequencies, a straight line results in an angle of 45° to the real axis and, at lower frequencies, the slope suddenly increases but does not change to a vertical line [16].

## II.5.14 Semiconductor Electrodes

The general scheme for a semiconductor electrode takes into account a two-step charge-transfer process [17]. One step corresponds to the transfer of electrons and ions through the Helmholtz layer. Let $Z_H$ be the corresponding impedance that is in parallel to $C_H$, the capacity of the Helmholtz layer and let $Z_1$ be the impedance of this parallel combination. The other step exists due to the localization of charges in surface states or intermediates. Here the corresponding impedance, $Z_{sc}$, is in

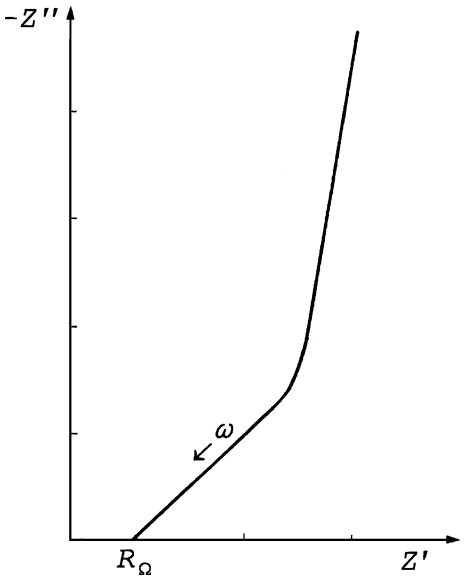


**Fig. II.5.7** Nyquist impedance plot due to a porous electrode with log-normal distribution of the pore sizes and with double-layer charging only

parallel to $C_{sc}$, the capacity of the depletion layer. Let $Z_2$ be the impedance of this parallel combination. The total impedance of the semiconductor electrode, $Z_{tot}$, results as $Z_{tot} = Z_1 + Z_2$. The quantity $(C_{sc})^{-2}$ plotting vs. the potential $V$ gives the Mott–Schottky plot. From this one can determine the flat-band potential of a semiconducting electrode [17].

## II.5.15 Kinetics of Non-Faradaic Electrode Processes

Let us now consider non-faradaic processes, i.e. kinetics of adsorption/desorption at electrodes without a charge transfer [1]. Here, the charge density $q_M$ is a function of both the electrode potential and the degree of coverage of the adsorbed substance. Sufficiently low frequencies result in the "thermodynamic" or "low-frequency capacity" $C_{LF}$, which is the sum of the "high-frequency capacity" $C_{HF} = (\mathrm{d}q_M/\mathrm{d}E)_{\Gamma,c}$ and a capacity, which is mainly determined by the potential dependence of the degree of coverage $\Theta$. This capacity leads to the occurrence of maxima in the capacity-potential dependence, i.e. at the potential of the adsorption/desorption maxima is the potential dependence of the degree of coverage maximal. If the adsorption process is too slow to follow the potential changes (for higher frequencies), non-capacitive behaviour can be observed, i.e. an adsorption admittance occurs. There are three main mechanisms of adsorption kinetics: first a diffusion control, second a control by the adsorption exchange rate and third a mixed control by diffusion and adsorption exchange.

Mixed adsorption–diffusion control was considered by Lorenz and Möckel [18], and they derived the following equations for the frequency-normalized admittance:

$$1/\omega R_{\mathrm{par}} = (C_{\mathrm{LF}} - C_{\mathrm{HF}}) \left((\omega\tau_{\mathrm{D}}/2)^{1/2} + \omega\tau_{\mathrm{A}}\right) \Big/ \left[\left((\omega\tau_{\mathrm{D}}/2)^{1/2} + \omega\tau_{\mathrm{A}}\right)^2 + \left((\omega\tau_{\mathrm{D}}/2)^{1/2} + 1\right)^2\right] \tag{II.5.46}$$

$$C_{\mathrm{par}} = C_{\mathrm{HF}} + (C_{\mathrm{LF}} - C_{\mathrm{HF}}) \left((\omega\tau_{\mathrm{D}}/2)^{1/2} + 1\right) \Big/ \left[\left((\omega\tau_{\mathrm{D}}/2)^{1/2} + \omega\tau_{\mathrm{A}}\right)^2 + \left((\omega\tau_{\mathrm{D}}/2)^{1/2} + 1\right)^2\right] \tag{II.5.47}$$

$$\tau_{\mathrm{D}} = (\mathrm{d}\Gamma/\mathrm{d}c)_{\mathrm{E}}^2 / D \tag{II.5.48}$$

$$\tau_{\mathrm{A}} = (\mathrm{d}\Gamma/\mathrm{d}\nu)_{\mathrm{E},c} \tag{II.5.49}$$

If the validity of the Frumkin adsorption isotherm is assumed, it follows that [19]

$$\tau_{\mathrm{D}} = \Gamma_{\mathrm{m}}^2 \Theta^2 (1-\Theta)^2 / \left[c^2 D (1 - 2a\Theta(1-\Theta))^2\right] \tag{II.5.50}$$

$$\tau_{\mathrm{A}} = \Gamma_{\mathrm{m}} \Theta (1-\Theta) / [\nu_0 (1 - 2a\Theta(1-\Theta))] \tag{II.5.51}$$

where $\Gamma_{\mathrm{m}}$ is the possible maximal surface concentration, $\Theta$ the degree of coverage, $c$ the bulk concentration of the surfactant, $D$ the diffusion coefficient of the surfactant, $a$ the Frumkin interaction coefficient, $\nu$ the adsorption rate and $\nu_0$ the adsorption exchange rate. This follows the general trend that $\tau_{\mathrm{D}}$ and $\tau_{\mathrm{A}}$ increase with increasing values of $a$. For $\Theta = 0.5$, the degree of coverage at adsorption/desorption potential and $a \to 2$ (two-dimensional condensation of the adsorption layer), it results that $\tau_{\mathrm{D}} \to \infty$ and $\tau_{\mathrm{A}} \to \infty$ . From this it follows that condensation of the adsorbed molecules leads to a complete loss of reversibility.

Equations (II.5.46) and (II.5.47) correspond to an equivalent circuit in which the capacity $C_{\mathrm{HF}}$ is in parallel with the adsorption impedance $Z_{\mathrm{A}}$. This impedance represents a series of an adsorption resistance (determined by the rate of adsorption) and a Warburg-like complex impedance (corresponding to diffusion of the surfactants) and a pure capacity $C_{\mathrm{LF}} - C_{\mathrm{HF}}$. The electrolyte resistance is already eliminated here. For very high frequencies, it follows that $C_{\mathrm{par}} = C_{\mathrm{HF}}$ and $Y''/\omega = 0$ and, for very low frequencies, results in $C_{\mathrm{par}} = C_{\mathrm{LF}}$ and $Y''/\omega = 0$. Figure II.5.8 shows the complex plane plots of the frequency-normalized admittance for adsorption control by exchange rate only (curve 1), adsorption control by diffusion only (curve 2), and adsorption control by exchange rate and diffusion (curve 3). Investigations of adsorption kinetics of sodium decyl sulphate were performed at the mercury/electrolyte interface using the frequency dependence of the electrode admittance at the potential of the more negative ad/desorption peak [20, 21]. It was concluded that diffusion control is the rate-determining step below and above the critical micelle concentration.

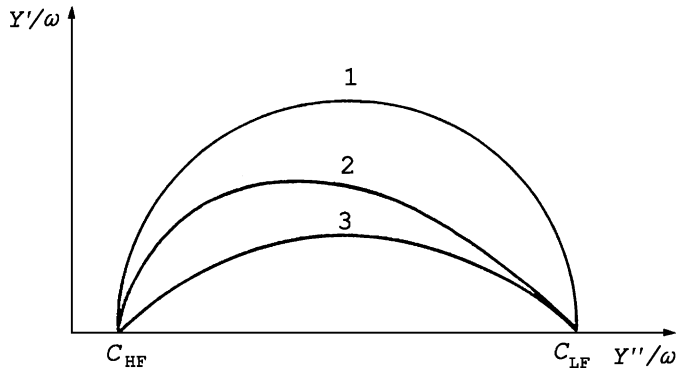


**Fig. II.5.8** Complex plane plot of the frequency normalized admittance. *Curve* 1 control by the adsorption exchange rate only; *curve* 2 control by diffusion only; *curve* 3 mixed control by the adsorption exchange rate and diffusion

Lorenz [22] considered the case that a two-dimensional association occurs in the adsorption layer. Here the surfactant monomers are in equilibrium with surfactant clusters of constant size. He derived the corresponding frequency dependence of cot $\delta_a = \omega C_{par} R_{par}$. For lower frequencies, a characteristic decrease in cot $\delta_a$ should appear compared to cot $\delta_a$ given by Eqs. (II.5.46) and (II.5.47). Such behaviour was in fact detected for higher concentrations of caproic as well as caprylic acid.

## II.5.16 References to Relevant Fields of Applications of EIS

– Corrosion, passive films [23–27]
– Polymer film electrodes [28]
– Characterization of electroactive polymer layers [29]
– Membrane systems [30]
– Solid electrolytes [31]
– Intercalation electrodes [32]
– Fuel cells research and development [33].

## References

1. Sluyters-Rehbach M, Sluyters J (1970) Sine wave methods in the study of electrode processes. In: Bard AJ (ed) Electroanalytical chemistry, vol 4. Marcel Dekker, New York, p 1
2. Gabrielli C (1990) Use and applications of electrochemical impedance techniques. Technical Report, Schlumberger Technologies
3. Schöne G, Wiesbeck W, Stoll M, Lorenz W (1987) Ber Bunsenges Phys Chem 91: 496
4. Brug G, van der Eeden A, Sluyters-Rehbach M, Sluyters J (1984) J Electroanal Chem 176: 275
5. Macdonald R (1987) Impedance spectroscopy. Wiley Interscience, New York

6. Marquard E (1963) J Appl Math 11: 431
7. Moré J (1978) Numerical analysis. In: Watson G (ed) Lecture notes in mathematics, vol 630. Springer, Berlin Heidelberg New York, p 105
8. Draper N, Smith H (1967) Applied regression analysis. John Wiley, New York
9. Brett CMA, Brett AM (1993) Electrochemistry – principles, methods, and applications. Oxford University Press, Oxford, pp 224–252
10. Sluyters-Rehbach M, Sluyters J (1984) A.C. techniques. In: Bockris J, Yeager E (eds) Comprehensive treatise of electrochemistry, vol 9. Plenum Press, New York, p 177
11. Vetter K (1952) Z Phys Chem (Leipzig) 199: 300
12. Jehring H, Retter U, Horn E (1983) J Electroanal Chem 149: 153
13. Kahlert H, Retter U, Lohse H, Siegler K, Scholz F (1998) J Phys Chem B 102: 8757
14. De Levie R (1967) Electrochemical response of porous and rough electrodes. In: Delahay P (ed) Advances in electrochemistry and electrochemical engineering, vol 6. Wiley Interscience, New York, p 329
15. Raistrick I (1990) Electrochim Acta 35: 1579
16. Song H, Jung Y, Lee K, Dao L (1999) Electrochim Acta 44: 3513
17. Gomes W, Vanmaekelbergh D (1996) Electrochim Acta 41: 967
18. Lorenz W, Möckel F (1956) Z Electrochem 60: 507
19. Retter U, Jehring H (1973) J Electroanal Chem 46: 375
20. Vollhardt D, Modrow U, Retter U, Jehring H, Siegler K (1981) J Electroanal Chem 125: 149
21. Vollhardt D, Retter U, Szulzewsky K, Jehring H, Lohse H, Siegler K (1981) J Electroanal Chem 125: 157
22. Lorenz W (1958) Z Elektrochem 62: 192
23. Armstrong R, Edmondson K (1973) Electrochim Acta 18: 937
24. Deflorian F, Fedrizzi L, Locaspi A, Bonora P (1993) Electrochim Acta 38: 1945
25. Gabrielli C (1995) Electrochemical impedance spectroscopy: principles, instrumentation, and application. In: Rubinstein I (ed) Physical electrochemistry. Marcel Dekker, New York, p 243
26. Mansfeld F, Lorenz W (1991) Electrochemical impedance spectroscopy (EIS): application in corrosion science and technology. In: Varma R, Selman J (eds) Techniques for characterization of electrodes and electrochemical processes. Wiley Interscience, New York, p 581
27. Mansfeld F, Shih H, Greene H, Tsai C (1993) Analysis of EIS data for common corrosion processes. In: Scully J, Silverman D, Kendig M (eds) Electrochemical impedance: analysis and interpretation. ASTM, Philadelphia, p 37
28. Lang G, Inzelt G (1999) Electrochim Acta 44: 2037
29. Musiani M (1990) Electrochim Acta 35: 1665
30. Buck R (1990) Electrochim Acta 35: 1609
31. Wagner J (1991) Techniques for the study of solid ionic conductors. In: Varma R, Selman J (eds) Techniques for characterization of electrodes and electrochemical processes. Wiley Interscience, New York, p 3
32. Metrot A, Harrach A (1993) Electrochim Acta 38: 2005
33. Selman J, Lin Y (1993) Electrochim Acta 38: 2063